Table VI. Quantification of Surface Atomic Ratios

compound	Si/N	N/Rh	Cl/Rh	Si/Rh
APS + $RhCl_3$	1.24	4.34	1.60	5.40
APS + D + $RhCl_3$	1.31	2.92	2.81	3.82
APS + B + $RhCl_3$ (10)[a]	1.34	3.92	3.31	5.26
APS + D + TEOS + $RhCl_3$ (12)[a]	4.88	3.12	3.02	15.21
APS + B + TEOS + $RhCl_3$ (9)[a]	12.66	0.85	3.09	10.71

[a] The numbers in parentheses correspond to compounds of Table III.

308.6–309.0 (about 1 eV lower) can be assigned to Rh^+ compounds (samples a–c); some of the samples (a, d, and e) show the presence of both oxidation states (Rh^{3+} and Rh^+), in agreement with the values given in the literature.[10]

The quantification of the surface atomic ratios (Table VI) agrees in some aspects with those calculated from the elemental analysis. Thus the N/Rh ratio in the samples of nonsupported complexes are quite similar (2.9 from XPS and 2.6 from elemental analysis in sample (APS + D + $RhCl_3$); 3.9 from XPS and 3.7 from elemental analysis in samples (APS + B + $RhCl_3$). Nevertheless, when the N functions are supported on hydrolyzed TEOS, the addition of $RhCl_3$ leaves the metal located mainly on the surface, and consequently the N/Rh ratio is lower (3.12 against 199, in sample 12, or 0.85 against 7.7, in sample 9). The Cl/Rh ratio varies in the range 1–3 in relation to the oxidation state of the metal.

Acknowledgment. This work was partially supported by the Comisión Interministerial de Ciencia y Tecnología, Spain (CICYT, project MAT88-0179C02-02) and by the Fundación Ramón Areces. We express our appreciation to Dr. J. L. Fierro for his help in the XPS studies. Grateful acknowledgement is also due to Dr. J. Sanz for the ^{13}C NMR spectra and to Dr. B. Casal for a critical reading of the manuscript.

Registry No. $(EtO)_4Si$, 78-10-4; $(EtO)_3Si(CH_2)_3NH_2$, 919-30-2; $PrNH_2$, 107-10-8; PhCOCOPh, 134-81-6; $CH_3COCOCH_3$, 431-03-8; NC_5H_4CHO, 1121-60-4; PrN=C(CH_3)C(CH_3)=NPr, 78788-23-5; PrN=C(Ph)C(Ph)=NPr, 136838-86-3; PrN=CH-2-py, 4206-52-4; SiO_2, 7631-86-9; $[RhCl(CO)_2]_2$, 14523-22-9; $[RhCl(COD)]_2$, 12092-47-6; $RhClCO(PEt_3)_2$, 14871-47-7.

Molecular Dynamics Simulation of the Temperature-Dependent Ionic Conductivity in Sodium(I)-β''-Alumina

Cathy Lane Rohrer† and Gregory C. Farrington*

Department of Materials Science and Engineering, University of Pennsylvania, 3231 Walnut Street, Philadelphia, Pennsylvania 19104

Received February 22, 1991. Revised Manuscript Received September 20, 1991

Molecular dynamics (MD) simulation has been applied to a study of structure, ion motion, and superlattice formation in the fast ion conductor, sodium(I)-β''-alumina. The results reproduce, in a general way, the curved variation of ionic conductivity with temperature observed in an Arrhenius-type plot of single-crystal conductivity data for the compound. The curvature in the conductivity plot may be explained as resulting from an evolution in the conduction mechanism from a vacancy mechanism at high temperatures to highly correlated superlattice motion at lower temperatures. A correlation is seen between the location of Mg(II) ions in the spinel blocks and the ion/vacancy arrangement in the conduction layers.

Introduction

Developing the ability to design materials with specified properties is an intriguing goal, one which may become more attainable with the growing accessibility of fast computers. To achieve this goal, however, computer models must be developed which accurately reproduce experimentally observed properties of known materials before they can be trusted as design tools. β''-Alumina is a particularly good material for testing such models. Well-known for its ability to undergo ion exchange with a variety of mono-, di-, and trivalent cations, β''-alumina exhibits varied optical, structural, and transport properties depending on its mobile cation composition. It represents a good beginning challenge for simulation, since its composition and properties can be varied extensively without altering its structural framework. A reasonable computer model for β''-alumina should be able to reproduce the properties of its isomorphs.

This paper presents a study of the temperature-dependent ionic conductivity of pure sodium(I)-β''-alumina using molecular dynamics (MD) simulation. Prior studies of Na(I)-β''-alumina have shown that MD is effective as a structural probe, but its transport properties have not been accurately simulated for reasons both particular to the MD technique and to the structure of β''-alumina. For example, Wolf et al.[1] encountered the limitations of the MD technique in their study of Na(I)-β''-alumina. The MD technique enforces periodic boundaries on the system being simulated to avoid edge effects and more accurately represent long-range interatomic forces. Therefore, if the system under study has a tendency to order, as do the mobile ions in Na(I)-β''-alumina, the periodicity imposed by the MD technique must match the periodicity of the ordering under consideration. Otherwise, the MD-enforced periodicity will predominate over the system periodicity, and the atoms will never achieve an equilibrium configuration. As Wolf et al. noted in their work, their choice of MD "box" size, that is, the total number of unit cells explicitly included in the simulation, obstructed the mobile

† Current address: Alcoa, Alcoa Center, PA 15069-0001.

(1) Wolf, M. L.; Walker, J. R.; Catlow, C. R. A. *Solid State Ionics* **1984**, *13*, 33.

0897-4756/92/2804-0055$03.00/0 © 1992 American Chemical Society

cation ordering and, therefore, adversely affected their conductivity results at low temperatures where ordering has been experimentally observed to occur.

Zendejas et al.[2] overcame this problem by choosing a suitable number of unit cells to accommodate the expected Na(I) superlattice formation, which they were then able to reproduce. However, they did not attempt to calculate values of ionic conductivity. Had they done so, they would have encountered a second difficulty of the MD technique, its short time scale. Although the Na(I) conductivity of Na(I)–β''-alumina is quite high by normal standards, conductivity values are typically measured over a time scale of microseconds. In contrast, MD simulations generally last only several picoseconds, too short a time to obtain good jumping statistics from any but the most lively of cations. The simulation runs of Zendejas et al. lasted 5 ps and, as will be demonstrated in this work, were too short to observe the relatively slow correlated ion motion essential to modeling and understanding ion diffusion in Na(I)–β''-alumina.

Finally, neither Wolf et al. nor Zendejas et al. dealt with the fact that certain details of the structure of the β''-alumina spinel-type framework have not yet been established. In particular, while it is known that Mg(II) substitutes for Al(III) at tetrahedral sites in the framework to compensate for the charge of the excess Na(I) in the conduction layers, the exact locations of the individual Mg(II) cations are not known with certainty. Wolf et al. stated that Mg(II) had been included in their simulations, but did not say at which sites the Mg(II) ions had been placed. Zendejas et al. simulated only one-third of the β''-alumina unit cell, sacrificing distance along the c axis in order to expand the a–b plane while avoiding an unwieldy number of atoms. By doing so, they were forced to disregard the Mg(II) sites altogether.

The work presented here addresses both the technical difficulties of the MD simulation technique and the particular challenges of applying it to the study of the β''-aluminas. The results show that it is possible to reproduce experimental conductivity values in β''-alumina by MD simulation and provide rich insight into the micromechanisms of ion motion in this fast ion conductor. However, they do not suggest that it should be possible to predict whether or not a hypothetical compound is a good ionic conductor, since the successful simulation of the details of the fast ion motion in Na(I)–β''-alumina requires that considerable supporting information be known about the compound a priori.

Structural Background

Na(I)–β''-alumina is a layered oxide with the chemical composition $Na_{1+x}Mg_xAl_{11-x}O_{17}$, where x is typically 0.67. The structure, as determined by Yamaguchi and Suzuki[3] and Bettman and Peters,[4] is comprised of alternating layers of spinel-type blocks and conduction layers. The spinel blocks, so-called because of their structural similarity to the mineral spinel, consist of four close-packed oxygen layers with aluminum cations at the tetrahedral and octahedral interstitial sites. The conduction layers are made up of "column" oxygens and contain the entire sodium content of the compound. The column oxygens link aluminums at tetrahedral sites in the spinel blocks bordering the conduction layers and thus form Al–O–Al columns which serve as supports for the β''-alumina framework. The excess sodium in the conduction layers, indicated by the nonstoichiometric chemical formula for the material, is charge compensated by Mg(II) substitution for Al(III) in the spinel blocks.

As mentioned previously, exactly where the Mg(II) substitution occurs is still somewhat of a mystery. The magnesium distribution is important because it is expected to affect the location of the sodium cations in the conduction layers and, thus, the cation-transport mechanism. Neutron diffraction can distinguish between magnesium and aluminum but only yields average structural information. Frase et al.[5] carried out single-crystal neutron diffraction refinements of the structure of Na(I)–β''-alumina and reported that the magnesium content does not vary with sodium content as assumed by the chemical formula given previously for Na(I)–β''-alumina. Rather, they reported that Mg(II) and Al(III) species alternate in the tetrahedral aluminum sites (Al(2) sites) at the centers of the spinel blocks, half the Al(III) having been replaced by Mg(II). This mechanism compensates for some but not all of the charge of the excess sodium. The remaining charge, according to this model, is compensated by aluminum vacancies.

The results of Frase et al. are not consistent with previous work of Roth et al.,[6] who found no vacancies in the spinel blocks using neutron diffraction. They reported 38% Mg(II) occupancy of the Al(2) sites and 4% occupancy of the tetrahedral Al(4) sites which are closer to the conduction layers. Since diffraction gives only average structural information, no attempt was made to determine whether the magnesium was distributed randomly over these sites or in an ordered fashion.

On the basis of still another study of the structure of Na(I)–β''-alumina using neutron diffraction, Alden et al.[7] have suggested that the Mg(II) ions are distributed in domains and are ordered over the Al(2) sites but to a lesser extent in a sample that had been held at 1350 °C and subsequently quenched. They suggested that a more random distribution of Mg(II) in the quenched sample might lead to higher Na(I) conductivity in the conduction layers.

It is clear from these different models that a good understanding of how Mg(II) is distributed in the spinel blocks would be useful for understanding the distribution and transport mechanisms of the mobile cations in the conduction layers.

Another distribution of importance is that of the mobile cations. The average mobile cation distribution in Na(I)–β''-alumina has been determined by X-ray diffraction, although β''-alumina's high ionic conductivity leads to large thermal parameters and subsequent difficulty in determining exact site occupancies in the conduction layers. Generally, the mobile cations are free to move along hexagonal pathways around the column oxygens. The most preferred site along these pathways for Na(I) is the tetrahedrally coordinated Beevers–Ross (BR) site, located at the hexagon corners. In $Na_{1.67}Mg_{0.67}Al_{10.33}O_{17}$, there are five mobile cations for every six BR sites, leaving one out of six BR sites vacant.

This high number of vacancies has led to the generally accepted belief that ion transport in Na(I)–β''-alumina occurs by a vacancy mechansim. However, an Arrhenius-type plot of the Na(I) conductivity in β''-alumina, a typical example of which is shown in Figure 1, indicates

(2) Zendejas, M. A.; Thomas, J. O. *Solid State Ionics* **1988**, *28*, *30*, 46.
(3) Yamaguchi, G.; Suzuki, K. *Bull. Chem. Soc. Jpn.* **1968**, *41*, 93.
(4) Bettman, M.; Pters, C. R. *J. Phys. Chem.* **1969**, *73*, 1774.
(5) Frase, K. G.; Thomas, J. O.; Farrington, G. C. *Solid State Ionics* **1983**, *9*, *10*, 307.
(6) Roth, W. L.; Reidinger, F.; LaPlaca, S. In *Superionic Conductors*; Mahan, G. D., Roth, W. L., Eds.; Plenum Press: New York, 1976.
(7) Alden, M.; Thomas, J. O.; Davies, P. *Solid State Ionics* **1986**, *18*, *19*, 694.

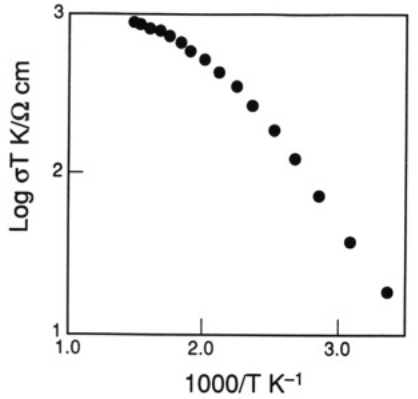

Figure 1. Ionic conductivity in Na(I)-β″-alumina.

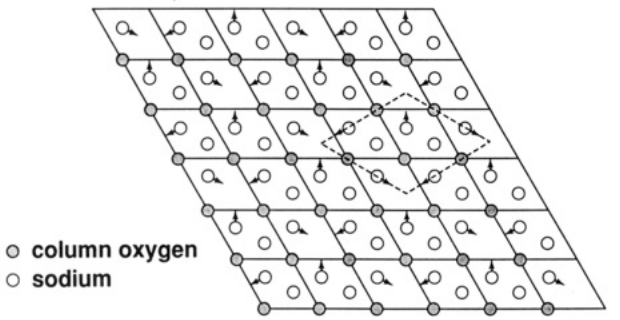

Figure 2. Schematic diagram of the $\sqrt{3}a$ by $\sqrt{3}a$ superlattice formation at low temperatures in Na(I)-β″-alumina. Arrows indicate the direction of Na(I) relaxation toward neighboring vacancies.

that the transport mechanism may not be quite so simple. As can be seen in the figure, there is a pronounced curvature in the temperature dependent conductivity in the vicinity of 300 °C. Briant and Farrington[8] conjectured that this nonlinearity is a result of an order/disorder transition from low to high temperatures. In fact, ordering at low temperatures has been observed by Boilot et al.[9] using diffuse X-ray scattering. They observed extra diffraction spots which indicate the formation of a $\sqrt{3}a$ by $\sqrt{3}a$ superlattice in the conduction layers. A schematic representation of this superlattice is shown in Figure 2.

Simulation Techniques

For a thorough discussion of the MD technique, we refer the reader to the work of Sangster and Dixon.[10] This section presents details of the MD technique particular to this study.

The potential energy used in our MD code, loosely based on the code FUNGUS,[11] is in the Born–Mayer–Huggins form. Short-range interatomic potentials were taken from Walker et al.[12] and are the same potentials used in the work of Wolf et al.[1] and Zendejas et al.[2] The Mg–O potential was taken from the work of Lewis.[13] Long-range Coulombic interactions were calculated by Ewald summation.

The original version of FUNGUS conserved volume, number, and energy. In this form, it was not appropriate for our research problem which was to study temperature-dependent properties obviously involving variations in volume. Therefore, the code was modified to allow for volume relaxation during the standard equilibration period. Equilibration typically involves scaling the atomic velocities to achieve a desired temperature. In the modified code, the lattice parameters were also scaled to achieve a negligible internal pressure or stress. The stress tensor is equivalent to the force of the atoms on the simulation box, and its components are calculated as follows:[14]

$$\tau_{ab} = (1/\Omega)\{\sum_i m_i v_{ia} v_{ib} + \sum_i \sum_{j>i} (r_{ija} \cdot F_{ijb})\}$$

Here, Ω is the volume of the simulation box, a and b range over the x, y, and z directions, and the summations are over all of the atoms in the system. The hydrostatic pressure is calculated as $^1/_3(\tau_{xx} + \tau_{yy} + \tau_{zz})$.

The lattice parameter scaling was carried out under the simple assumptions that the change in total volume should be proportional to the hydrostatic pressure and that the change in c lattice parameter should be proportional to the diagonal component in the z direction of the internal stress tensor. The simulation box volume, the c lattice parameter, and subsequently, by simple geometry, the a lattice parameter were then periodically adjusted until all of the stress tensor elements were negligible. The lattice parameters at this point were taken as the equilibrium values and were held constant for the rest of the simulation run. Note that the rhombohedral symmetry of the box was not allowed to change.

Equilibration was complete within 1000–4000 time steps, depending on the size of the simulation box. The total energy remained stable after equilibration, fluctuating approximately ±0.02% around average. A 2000 time step simulation run of 18 full unit cells used 1.5 h of computer time on the Pittsburgh Supercomputing Center Cray Y-MP.

Influence of the Mg(II) Distribution on Conductivity

Noting that the size of the simulation "box" can greatly influence simulation results, we felt it necessary to explore the influence of varying the structural input, especially in light of the undetermined Mg(II) distribution in β″-alumina. Although MD simulations are not well suited to determine the correct Mg(II) distribution in the spinel blocks, they are suited to probing the relationship between a given Mg(II) distribution and the Na(I) distribution in the conduction layers. To this end, several simulations were carried out, the first of which were highly unphysical in that only one-third of the unit cell was used. This approach is similar to that of Zendejas et al.,[2] except for the way in which the cell was truncated. In this work, one full conduction layer and one full spinel block were incorporated, as shown in Figure 3. The MD technique then enforced three-dimensional periodic boundaries, thus removing the 3-fold screw axis in the c direction which is present in the real crystal and making the Mg(II) distribution above and below the single conduction layer unnaturally symmetric. Although the total crystal symmetry was, therefore, lost by this truncation, the local environments above and below the conduction layer were kept intact, as shown in the figure. Zendejas et al. truncated their spinel blocks at the oxygen layer before the central tetrahedral and octahedral Al(III) sites (the Al(2) and Al(1) sites), filled the remainder of the unit cell with vacuum, and held their outer oxygen layers fixed for the duration of their simulations. In contrast, all atoms in our work were free to move.

(8) Briant, J.; Farrington, G. C. *J. Solid State Chem.* **1980**, *33*, 385.
(9) Boilot, J. P.; Collin, G.; Colomban, Ph.; Comes, R. *Phys. Rev. B* **1980**, *22*, 12.
(10) Sangster, M. J. L.; Dixon, M. *Adv. Phys.* **1976**, *25*, 247.
(11) Walker, J. R. In *Computer Simulation of Solids, 166, Lecture Notes in Physics*; Catlow, C. R. A., Mackrodt, W. C., Eds.; Springer: Berlin, 1982.
(12) Walker, J. R., Catlow, C. R. A. *J. Phys. C* **1982**, *15*, 6151.
(13) Lewis, G. V. *Physica* **1985**, *131*, 114.
(14) Allen, M. P.; Tildesley, D. J. *Computer Simulation of Liquids*; Oxford University Press: New York, 1987.

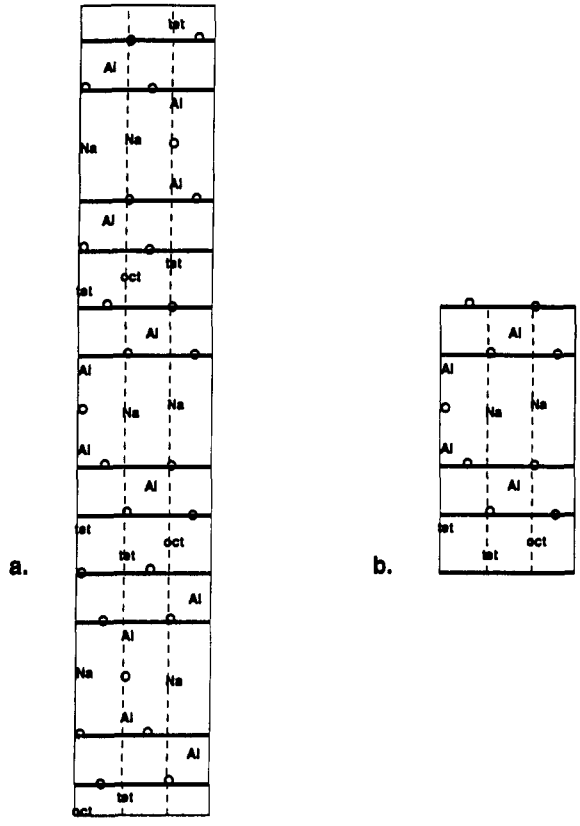

Figure 3. One-third unit cell segment used to test the influence of the Mg(II) distribution on the Na(I) distribution. (a) Full unit cell sliced along the (11l) plane. (b) One-third unit cell used in Mg(II) distribution tests. Bold horizontal bars represent close-packed oxygen layers. tet and oct mark the central tetrahedral (Al(2)) and octahedral (Al(1)) Al(III) sites in the spinel blocks. Dashed lines are drawn through these sites to show their relationship to the mobile cations in the conduction layers.

Three different Mg(II) distributions were then tested using a box size of 36 truncated unit cells: (1) a 2a by 3a pattern over the Al(2) sites above and below BR sites, (2) a random pattern over these BR-related sites, and (3) a 2a by 3a pattern over the other Al(2) site which lies above and below column oxygens. Figure 3 shows the relationship of these Al(2) sites to the conduction layer sites. (Note that the Al(2) site related to the column oxygen actually becomes octahedrally coordinated when the unit cell is truncated, as a result of the unphysical periodicity in the z direction.) The Mg(II) distributions viewed down the c axis are shown schematically in Figure 4a–c. The two Al(2) sites are shown in the same plane in this figure so that the Mg(II) distributions can be seen more clearly, but they are actually skewed, as shown more accurately in Figure 3.

Volume relaxation was not carried out for these tests, but the same lattice parameters were used for each. Each system was equilibrated at 400 °C for 500 times steps and 300 °C for an additional 1000 time steps and then allowed to run at 300 °C for 5000 time steps (25 ps). The purpose of the initially higher temperature equilibration period was to give the mobile cations enough kinetic energy to move out of the probably nonequilibrium sites at which they were initially placed. The temperature was subsequently decreased to a temperature near the order/disorder transition temperature, thus possibly affording the opportunity to demonstrate the Mg(II) influence on Na(I) conductivity and correlation.

As can be seen in Figure 4d,e, the two systems with Mg(II) in BR-related Al(2) sites resulted in a Na(I) distribution which exactly mimicked the Mg(II) distribution. This result is reasonable since one might expect that the Na(I) cations would seek the lower charged Mg(II)-related sites while the vacancies would seek the higher charged Al(III)-related sites. The third system showed evidence of $\sqrt{3}a$ by $\sqrt{3}a$ superlattice formation, indicated in Figure 4f by the dashed lines. It is of interest that the third system was the only one to correctly reproduce the expected conduction layer structure, and it resulted in the lowest conductivity, the values being 0.128, 0.097, and 0.083 S/cm at 300 °C for the respective Mg(II) distributions. The experimental value at this temperature is approximately 1.26 S/cm. From these tests, it is apparent that the Mg(II) distribution does influence the mobile cation distribution despite the approximately 5-Å-thick spinel-type material which separates the Mg(II) ions from the conduction layers. However, a similar set of tests which used only nine truncated unit cells did not reveal any obvious relationship between the Mg(II) and Na(I) distributions. The superlattice formation always occurred, regardless of the Mg(II) positions. This result is most likely an artifact of the small box size. The nine unit cell box had the appropriate periodicity but was not quite big enough to encompass one full $\sqrt{3}a$ by $\sqrt{3}a$ superlattice repeat unit.

Hoping to obtain a better fit between the calculated Na(I) conductivity and experimental results, as well as to more realistically represent the crystal, our investigations next turned to simulations of full unit cells. Three new Mg(II) distributions were tested: (1) a $\sqrt{3}a$ by $\sqrt{3}a$ distribution over one of the two Al(2) sites; (2) a 2a by 3a distribution over the same sites; (3) a random distribution over both Al(2) sites. Again, a 36 unit cell box was used, this time containing 3204 atoms. All three systems were allowed to equilibrate until their respective volumes no longer changed, and then the volumes were held constant while the temperature alone was allowed to stabilize at 350 °C for 500 more time steps of 3.5×10^{-15} s each. The resulting unit cell volumes were between 923 and 925 Å^3.

As with the truncated unit cells, the resulting conductivity values differed. Calculated over 16.8 ps or 4800 time steps, the values were 0.496, 0.303, and 0.267 S/cm, respectively, at 350 °C. The experimental value at 350 °C is approximately 1.30 S/cm. However, now that the Mg(II) distributions were no longer symmetrical above and below the conduction layers, their influence on the Na(I) distributions was not as pronounced. Evidence of $\sqrt{3}a$ by $\sqrt{3}a$ superlattice formation among the sodium ions was observed in all three systems at some point during the simulation runs, and it is of interest that in the first two systems, the vacancies in these superlattice formations always fell between central octahedral Al(III) sites in one spinel block and the set of central tetrahedral Al(III) sites in the other spinel block at which no Mg(II) was substituted. This did not hold true in the disordered system since the Mg(II) was scattered over both Al(2) sites. Furthermore, the disordered system exhibited an increasing drift in temperature, indicating that it was not a stable configuration. Because the $\sqrt{3}a$ by $\sqrt{3}a$ Mg(II) distribution seemed the logical first guess for the real structure given the reported Na(I) ordering, this distribution was chosen for the temperature-dependent simulations. It is unclear why the calculated conductivity values are lower than the experimental values, but statistical limitations due to the small number of mobile cations and the short simulation time scale are likely causes.

Temperature-Dependent Simulation Results

Three attempts at simulating the temperature depen-

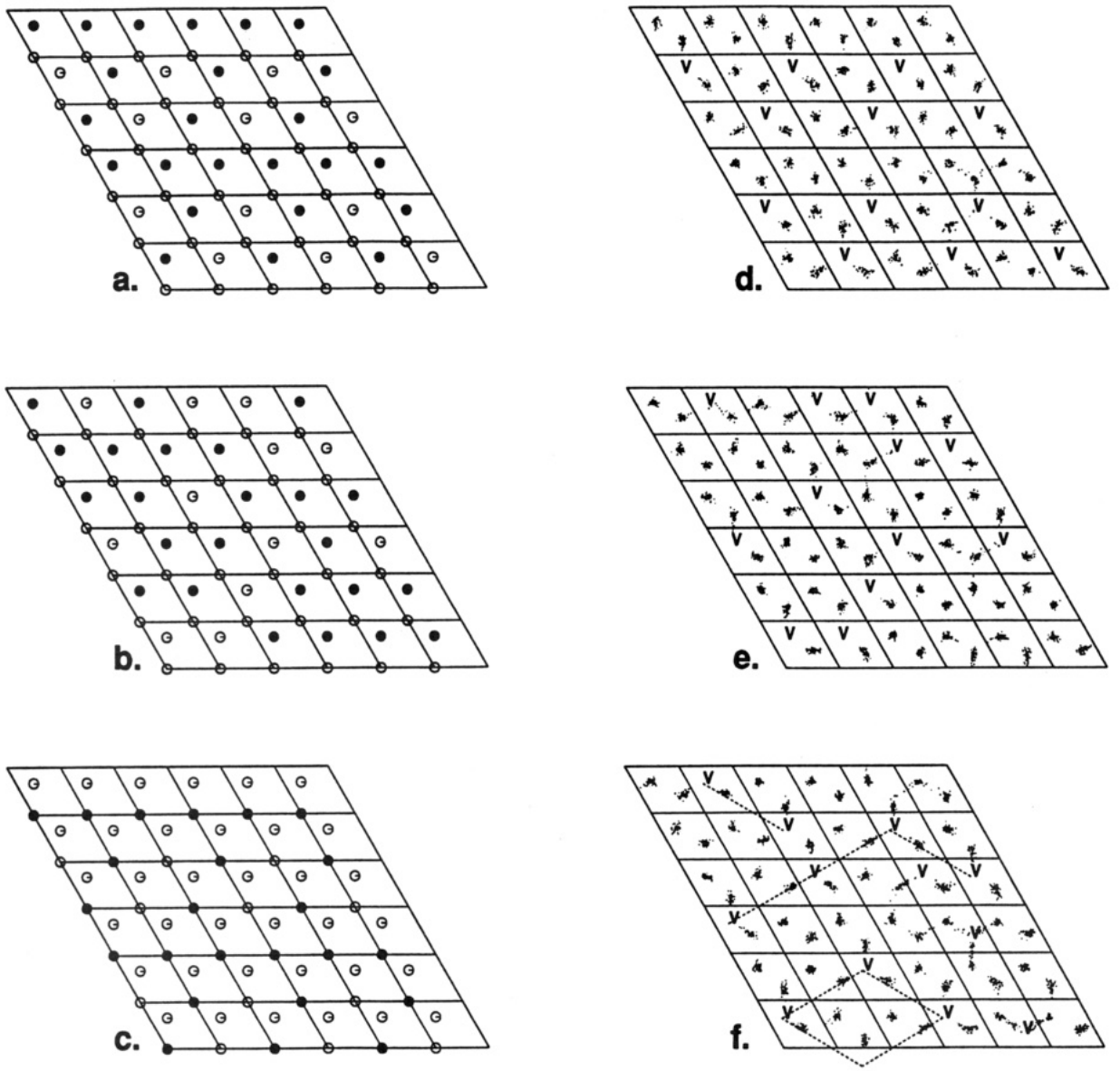

Figure 4. Correlation between Mg(II) distribution and Na(I) distribution in simulations of one conduction layer and one spinel block of Na(I)–β″-alumina. Solid circles, Mg(II); open circles, Al(III); V, vacancies. (a) Mg(II) ordered in a 2*a* by 3*a* pattern over the BR site-related Al(2) sites. (b) Mg(II) randomly distributed over these sites. (c) Mg(II) ordered in a 2*a* by 3*a* pattern over the column oxygen-related Al(2) sites. (d)–(f) 5.6-ps snapshots of the Na(I) trajectories corresponding to (a)–(c), respectively. Column oxygens are not shown.

dence of the transport properties in a nine unit cell box were carried out in which only the initial positions of the mobile cations were changed. In all three cases, the Mg(II) was distributed randomly over one of the two Al(2) sites, since the truncated nine unit cell Mg(II) tests mentioned in the previous section indicated that the Mg(II) placement had no apparent effect on the conduction layers. Thus, a 3*a* by 3*a* periodicity was enforced by the choice of the box size. All three cases became unstable at low temperatures in the sense that spinel block atoms moved too far from their crystallographic sites, which is possibly related to the use of incorrect Mg(II) distributions. The highest starting temperature was 700 °C, and the lowest temperature attained before the simulation runs became unstable was 200 °C. Conductivity values were of the correct order of magnitude, as shown in Figure 5, but did not reproduce the experimentally observed trend as the temperature decreased. It is interesting to note, however, that the $\sqrt{3}a$ by $\sqrt{3}a$ superlattice was observed in the lower temperature runs and that it was apparently mobile. In fact, highly correlated mobile cation jumps were observed, always maintaining the superlattice formation.

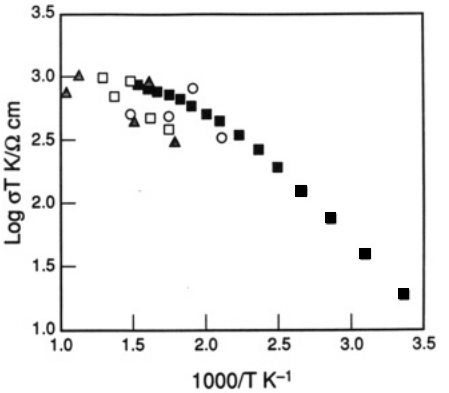

Figure 5. Conductivity results of three 9 unit cell simulations of Na(I)–β″-alumina. Solid squares represent experimental results (see Figure 1).

To check whether this correlated motion of the mobile cations was dependent on the box size and to adjust the

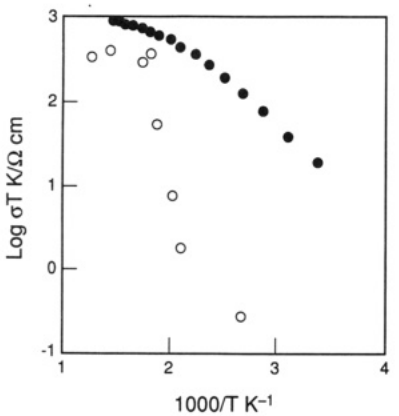

Figure 6. Temperature-dependent conductivity results from an 18 unit cell simulation of Na(I)–β''-alumina.

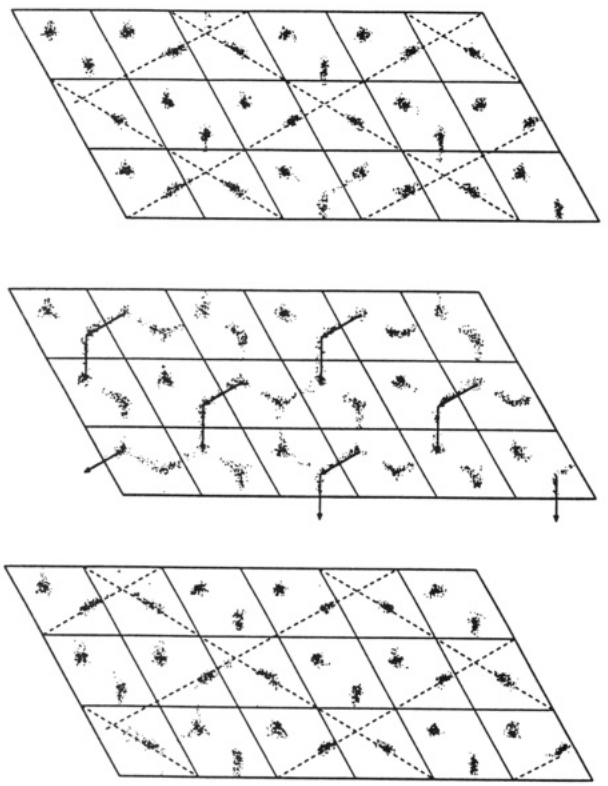

Figure 7. Sequential 7 ps snapshots of the Na(I) trajectories at 250 °C. Arrows indicate cation jumps. Dashed lines mark the vacancy superlattice formation. Column oxygens are not shown.

Mg(II) distribution, simulations of an 18 unit cell box were carried out with the Mg(II) arranged in a $\sqrt{3}a$ by $\sqrt{3}a$ pattern over one of the two Al(2) sites, as discussed earlier. These simulations were started at 600 °C and continued down to room temperature. At each temperature, the volume was allowed to relax until it no longer changed, and then the system was run freely for 6000 time steps of length 3.5×10^{-15} s each. The starting configuration of the mobile Na(I) cations at each lower temperature was taken from the reboxed final positions of the previous higher temperature run. The system was stable at all temperatures measured.

The resulting conductivity as a function of temperature is shown in Figure 6. As the temperature was decreased, the $\sqrt{3}a$ by $\sqrt{3}a$ vacancy superlattice became more prevalent, until it remained fixed over the 21-ps duration of the simulations at the lowest temperatures measured. Of particular interest is the fact that as in the full unit cell Mg(II) distribution tests, the vacancy superlattice was

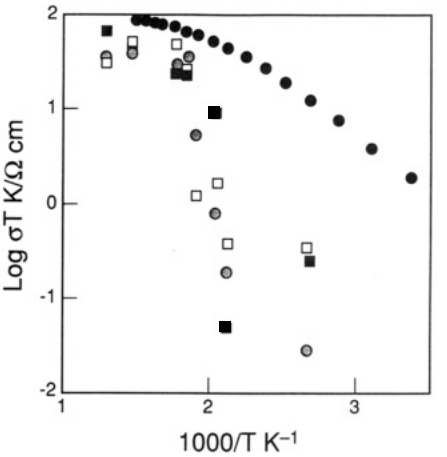

Figure 8. Comparison of simulated temperature-dependent conductivity values after 7 ps (white squares), 14 ps (grey circles), and 21 ps (black squares). Black circles represent experimental results.

Table I. Number of Na(I) Jumps Completed as a Function of Temperature in an 18 Unit Cell Simulation of Na(I)–β''-Alumina

temp, °C	7 ps	14 ps	21 ps	total
500	52	83	95	230
400	53	43	62	158
300	51	26	22	99
200	29	45	5	79
100	3	6	2	11

correlated with the Mg(II) distribution in that the vacancies always fell between Al(III)-filled octahedral and tetrahedral sites. Furthermore, as in the nine unit cell simulations, the vacancy superlattice at low temperatures was apparently mobile. This can be seen in the sequential, 7-ps snapshots of the Na(I) trajectories in one conduction layer at 250 °C shown in Figure 7.

The agreement between the transport behavior in the 9 and 18 unit cell boxes indicates either that the correlated motion is an artifact of the small box sizes used or that this motion is real and perhaps explains the higher activation energy for ionic conductivity that has been experimentally observed at low temperatures. The argument against this correlated behavior being a box artifact is that the superlattice motion was clearly observed in only one of the three conduction layers. The fact that it was observed at all was rather fortuitous in that the breaks in the simulation runs, necessitated by an overabundance of data after too many time steps, coincided with the periods of relative ionic stillness and motion in that particular conduction layer. Whether these periods were offset, occurring at a different rate, or not occurring at all in the remaining conduction layers is unclear. If this behavior were a box effect, it seems likely that all three conduction layers would have been equally affected.

Finally, it is of interest that the simulated curvature in the conductivity plot occurs in approximately the correct temperature range, but the low-temperature activation energy is much too large. This can be partly attributed to the small time scale of the MD simulations. The conductivity values calculated after 2000, 4000, and 6000 time steps are shown in Figure 8. The high-temperature values are relatively stable since the Na(I) ions are quite mobile and the statistics are, therefore, quite good. As the temperature is decreased, however, fewer cations are moving, and the conductivity values are not as stable. This is exemplified by the differing number of jumps executed after specified time lengths, as listed in Table I. A jump was defined as completed when one mobile cation traveled

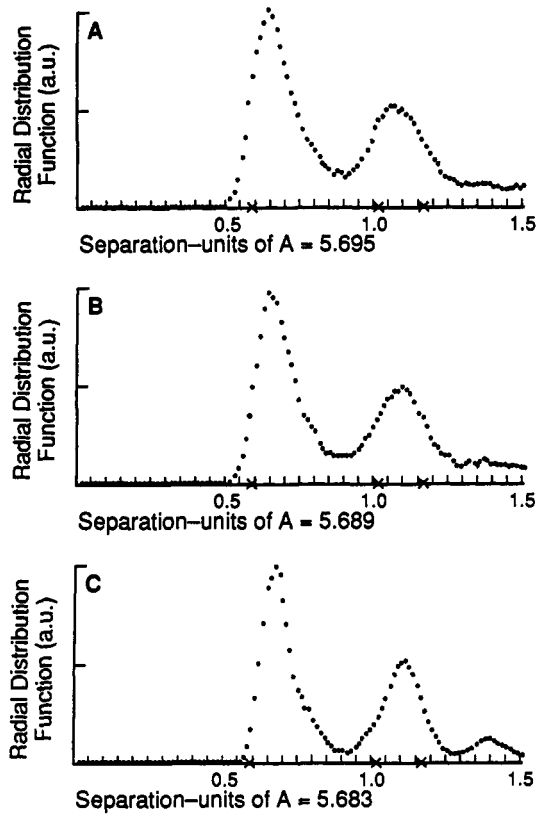

Figure 9. Na(I)–Na(I) radial distribution functions at (A) 500, (B) 300, and (C) 100 °C. The ×'s represent stoichiometric, crystallographic peak positions.

the crystallographic distance from one BR site to another.

These results focus attention on the question of how equilibrium is defined in MD simulations. Traditionally, a system is considered in equilibrium when its temperature and volume are stable, which is a definition based on energetic and structural considerations. Our results suggest that a better definition might be based on the stability of the principal phenomenon being simulated, in this case, conductivity. In β″-alumina simulations, energy and structure have equilibrated long before stable conductivity values are reached.

Moving from transport to structural properties, our simulations reconfirm the particularly good structural predictive capabilities of MD. Shown in Figure 9 are the simulated Na(I)–Na(I) radial distribution functions (rdf's) at 500, 300, and 100 °C taken from the 18 unit cell simulations. As expected, the peak widths decrease with decreasing temperature and the hump between the first and second nearest neighbors, indicative of the Na(I) relaxation toward neighboring vacancies as discussed in the work of Wolf et al.,[1] becomes more pronounced with decreasing temperature. In addition, the peaks are shifted from their stoichiometric, crystallographic locations, indicated by the ×'s marked on the horizontal axis. The rdf's agree quite well with those presented by Wolf et al.

One means of comparing simulated structure results to experimental results is to create atomic density maps. By superimposing the mobile cation trajectories from all three conduction layers and all unit cells, it is possible to produce average atomic density maps of the type created by neutron or X-ray diffraction refinements. Simulated density maps at 500, 300, and 100 °C are shown in Figure 10. As the temperature is decreased, the cations become more localized. As can be seen in the 100 °C simulation contour map, the two BR sites take on different occupations due to the superlattice formation. One site is either fully occupied or vacant, leading to the spherical occupation of the site at the corners of the rhombohedron in the figure. The other site is occupied by cations which are relaxed toward neighboring vacancies, leading to the more triangular occupation of the site at the ($^1/_3$, $^2/_3$) position. These contour maps agree quite well with those produced by the neutron diffraction refinements of Frase et al.[5] and with the superimposed Na(I) trajectories from the simulations of Zendejas et al.[2]

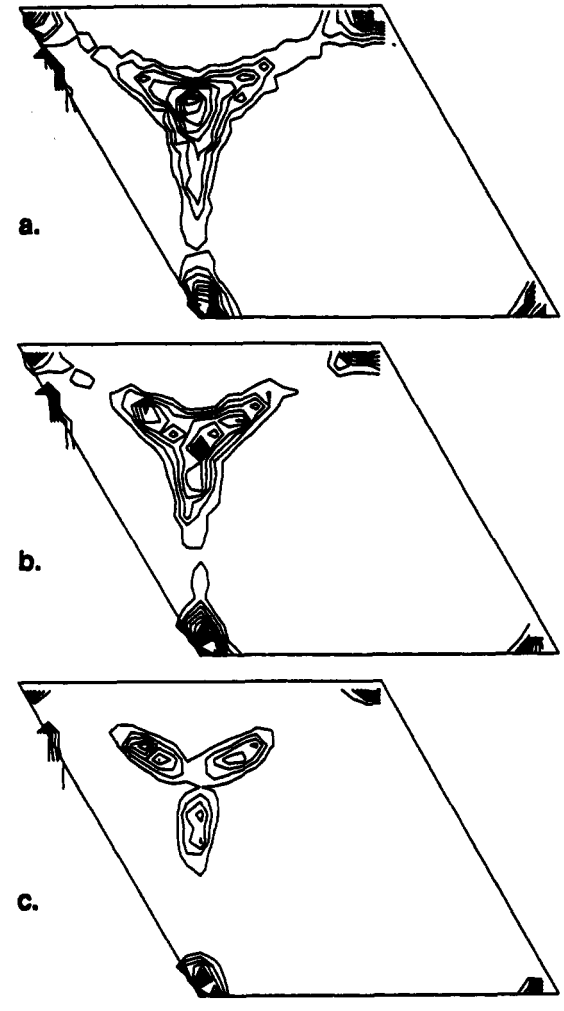

Figure 10. Simulated atomic density maps at (a) 500, (b) 300, and (c) 100 °C.

Finally, one can compare the simulated thermal expansion properties to experimental values. The calculated changes in lattice parameters with temperature for the 18 unit cell system were 2.77×10^{-5} and 1.52×10^{-4} Å/°C in the *a* and *c* directions, respectively, rather good matches for the experimental values of 4.56×10^{-5} and 2.34×10^{-4} Å/°C presented by May and Henderson.[17] It should be pointed out that the simulated magnitude of the *a* lattice parameter was 1% too large and the *c* lattice parameter 1% too small, although increasing the size of the MD box from nine unit cells to 18 unit cells improved the agreement.

Conclusions

It is clear that MD simulation can reproduce the bulk transport properties of Na(I)–β″-alumina. However, the

(15) Murch, G. E.; Thorn, R. J. *Philos. Mag.* **1977**, *36*, 529.
(16) Wolf, D. In *Fast Ion Transport in Solids*; Vashishta, P., Mundy, J. N., Shenoy, K., Eds.; Elsevier North Holland: Amsterdam, 1979.
(17) May, G. J.; Henderson, C. M. B. *J. Mater. Sci.* **1979**, *14*, 1229.

process of simulation is not as straightforward as might be wished. First there is the challenge of obtaining appropriate interatomic potentials. Fortunately, simple potential models which neglected polarizability worked well for the Na(I)-β''-alumina structure but will almost certainly be too simplistic for the simulation of more complex β''-aluminas, such as those in which the sodium content has been replaced by various divalent cations.

Then there are more subtle issues. For example, if ordering is known to occur in the system under study, information or at least an insightful guess about the superlattice repeat unit must be known a priori so as to avoid a simulation box size that will frustrate the ordering. Detailed knowledge of the crystal structure is also important. Although previously suggested in the literature, this work is the first to explicitly demonstrate that the Mg(II) distribution in the spinel blocks apparently does affect the placement and conductivity of the mobile Na(I). Unfortunately, MD does not provide a way of determining which Mg(II) distribution is correct, thus making the results obtained in this work valid only with respect to the chosen spinel configuration.

Finally, the simulations must be run for a long enough time to allow any correlated motion to be observed. Had the simulations of Na(I)-β''-alumina been run for only 1000 time steps, the low-temperature correlated motion observed after 6000 time steps would have been missed. Long simulations require plentiful computer time, which may not always be available. Nevertheless, once the groundwork is established and a generous computing facility located, MD can be an excellent aid to understanding experimental data. This is clear in our simulation results showing an apparent change in the mechanism of ionic conductivity in Na(I)-β''-alumina from a vacancy mechanism at high temperatures to highly correlated superlattice motion at lower temperatures.

Acknowledgment. This work was supported by the Office of Naval Research and the National Science Foundation, MRL program, under Grant No. DMR-8819885. All simulations were performed on the Pittsburgh Supercomputing Center Y-MP or a Stardent Titan provided by the Laboratory for Research on the Structure of Matter (NSF-MRL) at the University of Pennsylvania. We express our gratitude to M. Zendejas and J. O. Thomas for many useful discussions.

Registry No. Na(I)-β''-alumina, 110619-69-7; aluminum magnesium sodium oxide, 56780-19-9.

Lithium-MVO_5 (M = Nb, Ta) Bronzes

Jose-Manuel Amarilla,† Blanca Casal,† Juan-Carlos Galvan,‡ and Eduardo Ruiz-Hitzky*,†

Instituto de Ciencia de Materiales de Madrid, CSIC, Serrano 115 bis, 28006 Madrid, Spain, and Centro Nacional de Investigaciones Metalúrgicas, CSIC, Gregorio del Amo 8, 28040 Madrid, Spain

Received April 10, 1991. Revised Manuscript Received September 23, 1991

Mixed oxides $NbVO_5$ and $TaVO_5$ have been synthesized by a sol-gel procedure. Both compounds are isostructural with the so-called "monophosphate tungsten bronzes" (MPTB, $(PO_2)_4(WO_3)_{2m}$, with $m = 2$). In such structures single MO_4 tetrahedra (M = P, V), share corners with $M'O_6$ octahedra (M' = W, Ta, Nb) building pentagonal tunnels along the [010] direction. In this work, we have studied lithium insertion redox reactions carried out by treatments with LiI in acetonitrile in MVO_5 (M = Nb, Ta) hosts. Lithium insertion appears as a topotactic and reversible process. The intercalated compounds constitute a new family of Li bronzes showing Li_xMVO_5 compositions with $0 < x < 0.3$, which have been characterized by X-ray diffraction, conventional chemical analysis, and X-ray photoelectron spectroscopy. Complex impedance spectroscopy reveals the ionic character of the electrical conductivity in Li_xMVO_5. Typical values of the specific conductivity are in the 10^{-6}-10^{-8} Ω^{-1} cm^{-1} range at 573 K, with activation energies on the order of 0.5 eV.

Introduction

Transition-metal oxides are extensively applied as component materials in a wide diversity of electronic devices due to their semiconducting, superconducting, and ionic conducting properties. Of particular interest are those oxides able to act as host lattices for alkali-metal (Li, Na) ions, because they can be used as electrode materials in solid-state batteries and as specific sensors. Certain oxides in which the metal element have d^0 electronic configuration (i.e., group V metals) show intrinsic insulating or semiconducting properties, whereas partial reduction of the lattice and/or inclusion of electron donors (i.e., alkali-metal ions) into the host lattice can change drastically their electronic properties.[1] On the other hand, the coexistence of two or more metals in the composition of the oxide matrix can provide an advantage, because the associated electronic structure can improve the resulting properties with respect to those of the parent oxides.[2]

In a previous work,[3] we have shown the potential application of the sol-gel methods to the synthesis of a new crystalline phase in the system Nb-V-O, characterized as $NbVO_5$. We have extended this sol-gel method to the synthesis of $TaVO_5$, isostructural with $NbVO_5$, as discussed

† Instituto de Ciencia de Materiales de Madrid.
‡ Centro Nacional de Investigaciones Metalúrgicas.

(1) Rao, C. N. R.; Gopalakrishnan, J. *New Directions in Solid State Chemistry*; Cambridge solid state science series; Cambridge University Press: Cambridge 1986.
(2) Longo, J. M.; Horowitz, H. S. Solid State Synthesis of Complex Oxides. In *Preparation and Characterization of Materials*; Honig, Rao, Eds.; Academic Press: New York, 1981.
(3) Amarilla, J. M.; Casal, B.; Ruiz-Hitzky, E. *Mater. Lett.* 1989, *8*, 132.

0897-4756/92/2804-0062$03.00/0 © 1992 American Chemical Society